Journal of
NANOSTRUCTURES
JNS
NANOSTRUCTURES
JNS.kashanu.ac.ir

Synthesis of MWCNTs Using Monometallic and Bimetallic Combinations of Fe, Co and Ni Catalysts Supported on Nanometric SiC via TCVD

F. Shahi, M. Akbarzadeh Pasha*, A. A. Hosseini, Z. S. Arabshahi
Department of Solid state Physics, University of Mazandaran, Babolsar, 47416-95447, Iran.

Article history:
Received 26/04/2015
Accepted 18/05/2015
Published online 01/06/2015

Keywords:
MWCNTs
TCVD
Wet impregnation
Nanometric SiC
Monometallic catalyst
Bimetallic catalyst

**Corresponding author:*
E-mail address:
m.akbarzadeh@umz.ac.ir
Phone: 98 9190310503
Fax: +98 1135302480

Abstract

Nanometric Carbid Silicon (SiC) supported monometallic and bimetallic catalysts containing Fe, Co, Ni transition metals were prepared by wet impregnation method. Multiwall carbon nanotubes (MWCNTs) were synthesized over the prepared catalysts from catalytic decomposition of acetylene at 850°C by thermal chemical vapor deposition (TCVD) technique. The synthesized nanomaterials (catalysts and CNTs) were characterized by X-ray diffraction (XRD), Scanning Electron Microscopy (SEM), Transmission Electron Microscopy (TEM) and Raman spectroscopy. In this paper, using of nanometric SiC powder as catalyst support was examined and the effect of applied catalyst type on characteristics of grown CNTs was investigated. The results revealed that iron, cobalt and nickel are in oxide, cobalt ferrite ($CoFe_2O_4$) and nickel ferrite ($NiFe_2O_4$) forms and nanometric SiC powder can be applied as an appropriate catalyst support in CNT growth process. It was observed that the produced CNTs on bimetallic Fe-Co possess smaller average diameter, less amorphous carbon and denser morphology compared to other binary metallic combinations. It was found that the catalytic activity of bimetallic composition decreased in the order of Fe-Co> Fe-Ni> Co-Ni. Furthermore, the monometallic Fe catalyst has the most catalytic activity compared to monometallic Co and Ni catalysts.

1. Introduction

Carbon nanotubes represent one of the best examples of novel nanostructures that discovered in cathode deposits obtained in arc evaporation of graphite in 1991 by Ijima [1]. Due to its nanometer-sized tubular structure and the excellent physical, chemical, optical and magnetic properties the CNTs have wide applications in the fields of condensed matter physics and nanophase materials [2-4]. The techniques mainly used for the synthesis

of CNTs are arc discharge [5], laser ablation [6], and catalytic chemical vapor deposition [7, 8]. Among these methods CVD is the most versatile one because it can be used for production in large scale, enables the use of various substrates and allows CNT growth in a variety of forms [9]. The CVD growth of CNTs is a catalytic reaction. The Most commonly-used catalysts are transition metals; Fe, Co and Ni, because of two main reasons: (i) high solubility of carbon in these metals at high temperatures; and (ii) high carbon diffusion rate in these metals [10]. Cobalt, nickel, copper and zinc ferrites are important member of ferrite family and have excellent magnetic and electromagnetic properties. Considering the excellent properties of these ferrite nanoparticles as well as CNTs, the $M^{II}Fe_2O_4$ ((M^{II} = Co, Ni, Cu, Zn) decorated CNTs nanocomposite would be very attractive for many potential applications [11] Due to its wide-band gap semi-conducting feature, carbid silicon (SiC) may find extensive applications for high-temperature, high-frequency and high-power electronic. The combination of SiC and CNTs may create some new features for their future applications in electronic devices [12]. Murakami et al. reported their result of growing single-walled CNTs (SWCNTs) on SiC by CVD using ethanol as carbon source [13]. Multi-walled carbon nanotubes (MWCNTs) were grown on the surface of oxidized SiC whiskers by a xylene–ferrocene (carbon source-catalyst source) CVD process [12].

In this paper, we compare the effect of applying monometallic and bimetallic catalyst (Fe, Co and Ni) supported on nanometric SiC substrate by thermal chemical vapor deposition (TCVD) for CNTs synthesis.

2. Experimental procedure

2.1 Catalyst preparation

In this research, the starting materials were silicon carbide nanopowder (SiC, Beta, 99+ %) with particle sizes ranging from 45 to 65 nm (US Research Nanomaterials, Inc) and $Fe(NO_3)_3.9H_2O$ (supplied by Merck) and $Co(NO_3)_2.6H_2O$, (supplied by Merck) and $Ni(NO_3)_2.6H_2O$ (supplied by Aldrich). For catalyst preparation, the weight percentage of SiC substrate was kept constant at 80% and varying combinations of Fe, Co and Ni were tried and investigated. The designation, precursors, and composition of the six studied samples are given in table1.

Table 1. Designation, precursors, and composition of prepared catalyst samples.

Designation	Metal precursors	wt% of catalyst metal
2F	$Fe(NO_3)_3{\cdot}9H_2O$	20 % Fe
1F1C	$Fe(NO_3)_3{\cdot}9H_2O$ and $Co(NO_3)_2.6H_2O$	10% Fe + 10% Co
2C	$Co(NO_3)_2.6H_2O$	20 % Co
1C1N	$Co(NO_3)_2.6H_2O$ and $Ni(NO_3)_2.6H_2O$	10% Co + 10% Ni
2N	$Ni(NO_3)_2.6H_2O$	20 % Ni
1F1N	$Fe(NO_3)_3{\cdot}9H_2O$ and $Ni(NO_3)_2.6H_2O$	10% Fe + 10% Ni

The catalysts were prepared by wet impregnation method. 1 g SiC powder was dispersed in 20 ml of ethanol and stirred for 20 min in order to obtain a homogeneous suspension. An appropriate stoichiometric amount of $Fe(NO_3)_3{\cdot}9H_2O$, $Co(NO_3)_2.6H_2O$ and $Ni(NO_3)_2.6H_2O$ were solved in 5 ml distilled water separately and then were added gradually to the SiC suspension. The final mixture after 30 min stirring was dried at 80°C and calcinated at 800°C under air atmosphere for 2h and catalyst basis were obtained.

2.2 CNT synthesis

The synthesis of carbon nanotubes was carried out by a TCVD system using a horizontal tubular quartz reactor (length and diameter are 1200 mm and 50 mm, respectively) at atmospheric pressure. 50 mg of the prepared catalyst was disposed in a quartz boat and moved into the reactor. The precursor gas composed of acetylene and argon (C_2H_2/Ar = 15/150 Sccm) flows over the catalyst at 850°C for 15 minutes. After CNT synthesis the reactor was cooled down and the product (carbon deposit) formed along with the catalyst, was weighed and characterized. The carbon yield percentage and average growth rate of carbon deposit are calculated using the following equations, respectively [14]:

$$\text{Carbon yield}\,(\%) = \frac{M_{out} - M_{in}}{M_{in}} \times 100 \qquad (1)$$

$$\text{Average growth rate} = \frac{M_{out} - M_{in}}{\text{growth time}} \qquad (2)$$

Where M_{out} is the sum of the deposited carbon mass and catalyst mass after reaction, M_{in} the catalyst mass before reaction.

2.3 Materials characterization

The catalysts were characterized by X-ray diffraction (XRD). The phase and crystallinity of the compounds were identified by the position and intensity of characteristic peaks. The approximate sizes of metal particles (grain sizes) in the catalysts were estimated using the Scherrer equation by measuring the full width at half-maximum (FWHM) of the characteristic peak:

$$D = \frac{K\lambda}{\beta \cos\theta} \qquad (3)$$

where D is the approximate size of particle and K is the Scherrer constant, with the used value being 0.9, β is full width of half-maximum, λ is the wavelength of light used in the analysis which was λ=1.5406 Å and θ is the diffraction angle. The instrument used in the XRD analysis was a GBC diffractometer (Cu, kα, λ=1.5406 Å). The 2θ range of 10–90° was scanned at 0.04° per second. The morphology of CNTs was observed using Field Emission Scanning Electron Microscope (SEM, MIRA TESCAN) and Transmission Electron Microscopy (TEM, Zeiss - EM10C microscope working at 80 KV). Raman spectra of grown CNTs were recorded with Dispersive Raman Microscope SENTERRA BRUKER using a laser wavelength of 785 nm.

3. Results and discussion

The XRD patterns of the six catalysts supported on nanometric SiC are shown in Fig.1. It shows the representative peaks of SiC substrate, Fe_2O_3, Co_3O_4, NiO, $CoFe_2O_4$ and $NiFe_2O_4$ with different signs.

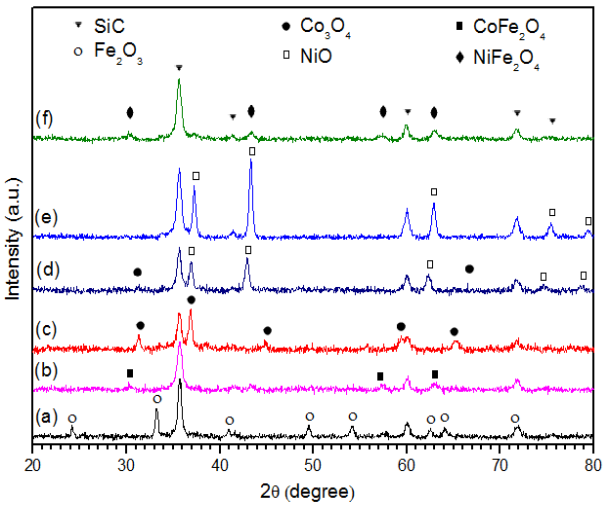

Fig. 1. XRD patterns of (a) 2F, (b) 1F1C, (c) 2C, (d) 1C1N, (e) 2N and (f) 1F1N catalytic samples.

The presence of iron oxide, cobalt oxide, nickel oxide, cobalt ferrite and nickel ferrite representative peaks in the XRD diagram of catalytic bases indicates that the chemical reactions in wet impregnation process have proceeded successfully to synthesize metal oxide catalyst particles from initial metal salt materials and also suggests that the temperature and time of calcination is appropriate. The silicon carbide has the β-SiC cubic crystal structure and for all catalyst samples, the most intense peaks observed at 2θ = 35.69°, 41.63°, 60°, 71.88°, 75.51° correspond to the SiC support.

The XRD analysis showed that the resultant Co_3O_4, $CoFe_2O_4$ and $NiFe_2O_4$ catalytic nanoparticles are in cubic structure and the Fe_2o_3, NiO ones possesses Hexagonal structure. Fig.1(d) and (e) show that in the bimetallic 1F1C and 1F1N catalysts, Cobalt ferrite ($CoFe_2O_4$) and Nickel ferrite ($NiFe_2O_4$) nanoparticles are formed.

Table 2. The approximate sizes of prepared catalytic nanoparticles**.**

Designation of catalyst	Metal Oxide	Catalyst nanoparticle size (nm)
2F	Fe_2O_3	25
1F1C	$CoFe_2O_4$	12
2C	Co_3O_4	23
1C1N	NiO	18
	Co_3O_4	20
2N	NiO	24
1F1N	$NiFe_2O_4$	15

The approximate sizes of catalytic nanoparticles are given in table2. Binary catalytic combination of Fe with Co and Ni produced smaller particles compared to combination of Ni and Co and both of these bimetallic possess smaller particles in comparison with their monometallic type which can be due to better dispersion of the metal particles over nanometric SiC in bimetallic catalyst types.

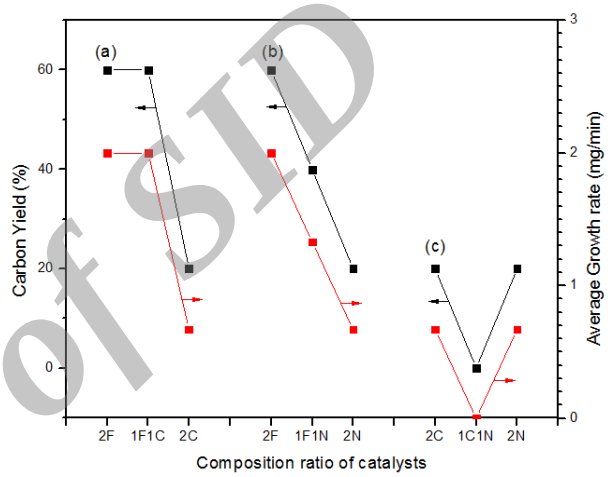

Fig. 2. Dependence of carbon yield and average growth rate of carbon deposit to catalytic composition: (a) Fe, Fe-Co, Co; (b) Fe, Fe-Ni, Ni; (c) Ni, Ni-Co, Co**.**

Fig.2 shows the carbon yield percentage and average growth rate of the prepared catalysts as a function of monometallic and bimetallic Fe, Co, Ni catalyst. The Fig.2(a) and (b) show that the carbon yield percentage decreases with increasing the ratio of Co and Ni to Fe content in the catalysts, respectively. The maximum yield and maximum average growth rate of the carbon product were observed for 2F and 1F1C catalysts. Fig.2(c) shows that carbon yield decreases in the bimetallic catalyst 1C1N with composition of 10% Co + 10% Ni. It suggests that Fe is more effective catalyst and has better catalytic activity on nanometric SiC substrate compared to Co and Ni.

Fig.3 shows the representative SEM images of grown CNTs on monometallic and bimetallic catalysts. Successful growth of CNTs on three types of prepared catalysts, confirms that the monometallic and bimetallic, Fe (Fig. 3a) Fe-Co (Fig. 3b), Fe-Ni (Fig. 3f) have suitable catalytic activity over nanometric SiC substrate, so that SiC powder can be applied as an appropriate catalyst support in CNTs production via thermal CVD.

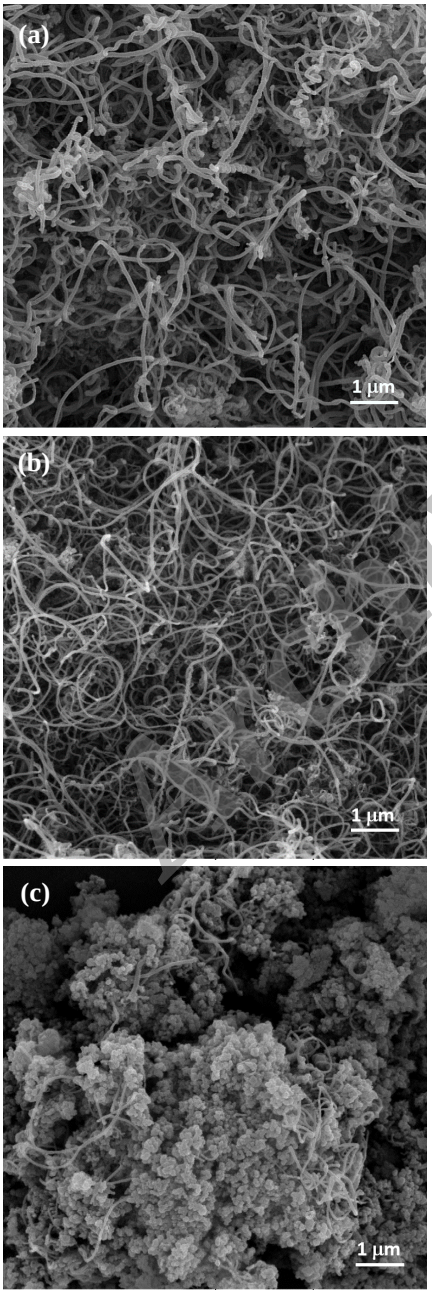

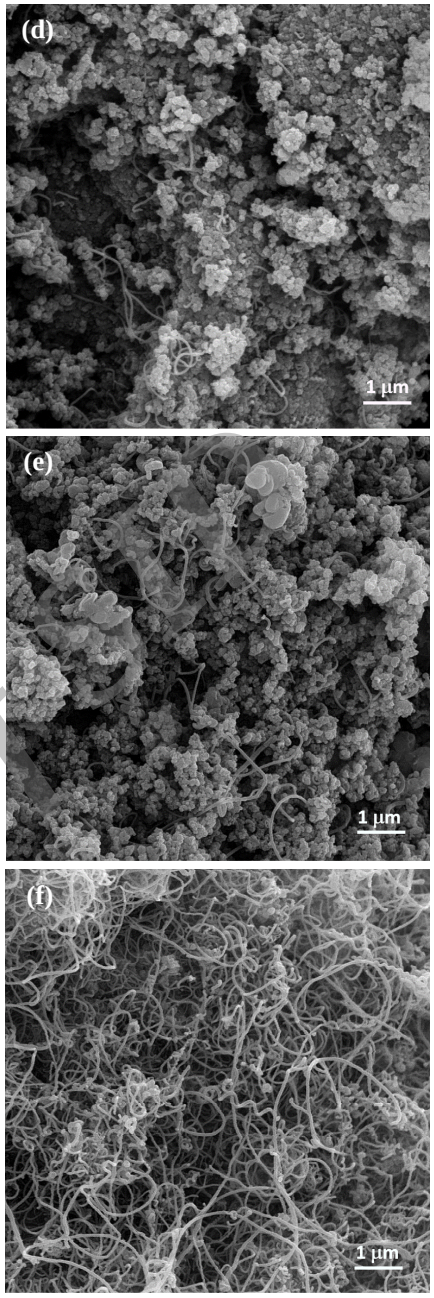

Fig. 3. SEM micrographs of grown CNTs on (a) 2F, (b) 1F1C, (c) 2C, (d) 1C1N, (e) 2N and (f) 1F1N catalysts.

Considering Fig.3(a), (b), (c) and Fig.3(a), (f), (e) (respectively related to (2F, 1F1C, 2C) and (2F, 1F1N, 2N) catalysts) it is obvious that the density of grown CNTs dramatically decreases when Co and Ni concentration exceeds Fe in catalyst

composition. On SiC support pure Co (Fig. 3c) and Ni (Fig. 3e) catalysts show very weak activity for catalyzing CNT growth compared to pure Fe (Fig. 3a). Moreover the activity of iron appears to be strongly affected by mixing it with cobalt and nickel. Image 3d shows that bimetallic catalyst Co-Ni is an inappropriate composition due to very low catalytic activities of monometallic Co and Ni catalysts.

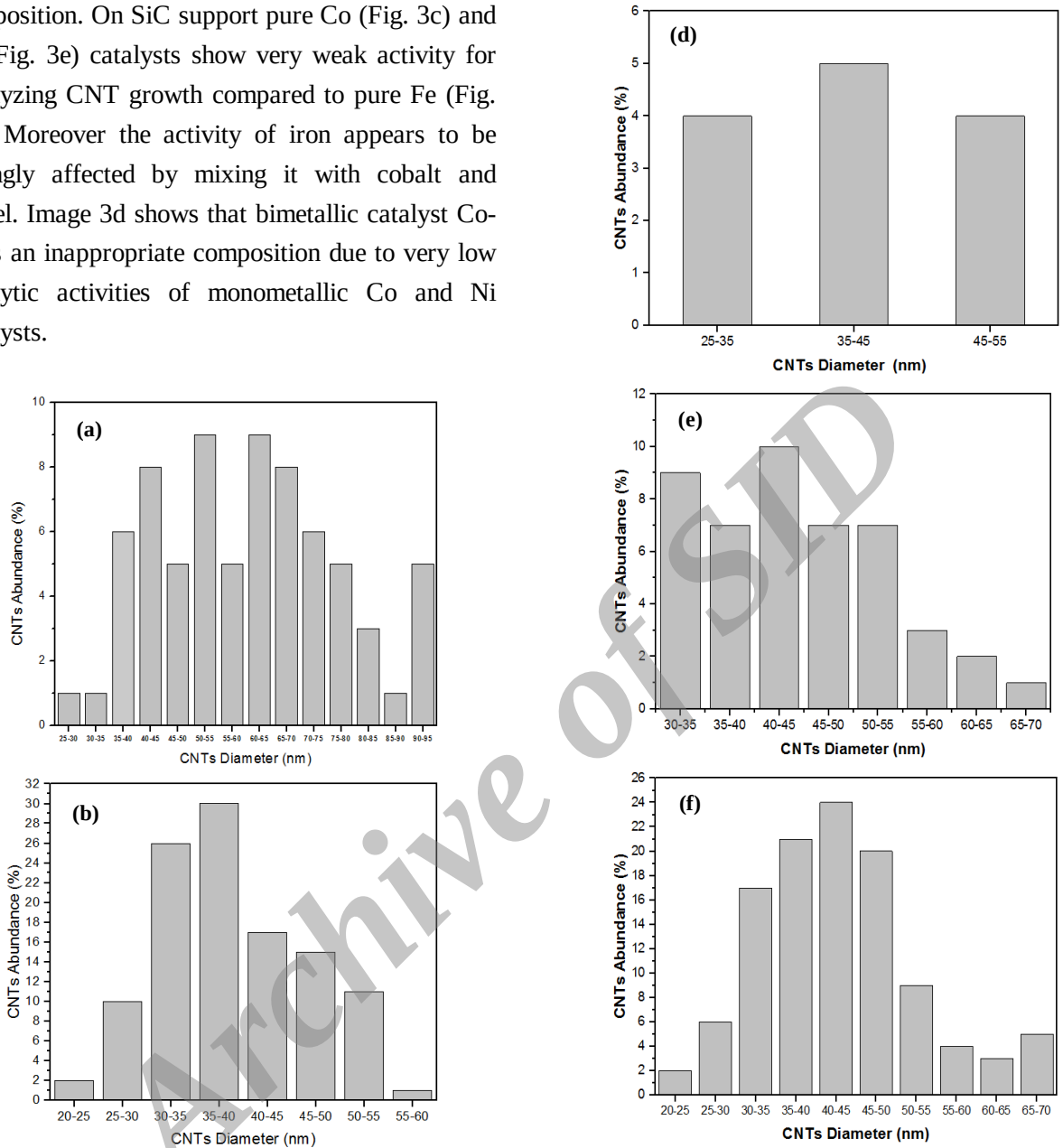

Fig. 4. Diameter distribution diagrams corresponding to SEM images of CNTs produced on (a) 2F, (b) 1F1C, (c) 2C, (d) 1C1N, (e) 2N, (F) 1F1N catalysts.

Statistical diameter distribution diagrams of grown CNTs are shown in Fig.4. The average diameters (AD) of CNTs obtained on different catalysts were reported in table3. The CNTs originated from the bimetallic 1F1C and 1F1N catalysts possess smaller average diameters

compared to other catalyst samples. In comparison between monometallic catalysts, the grown CNTs on Fe have denser structure, more homogeneous distribution and higher carbon yield and greater average diameter. Klinke et. al. tested Fe-, Co- and Ni-based catalysts on silica for CNT production with acetylene. They observed that iron produced the highest density of carbon structures at any considered temperature in the range of 580-1000°C [15]. Hernadi et. al. tested Fe- and Co-based catalysts with different hydrocarbons on various supports and observed that iron/silica presents the maximum activity in the decomposition of different unsaturated compounds [16]. Considering SEM observation beside carbon yield we can conclude that the best bimetallic catalyst composition for CNT production is 1F1C which has the best carbon yield and maximum amount of CNTs with smallest average diameter.

It seems that the presence of $CoFe_2O_4$ in the 1F1C catalyst increases its catalytic activity and improves its efficiency for CNT production. After this critical bimetallic catalytic composition, other good bimetallic catalyst is 1F1N, perhaps $NiFe_2O_4$ formation on this catalyst sample has increased its catalyst activity for carbon nanotube growth. Also the best monometallic catalyst is 2F catalyst (20% Fe).

Table 3. Average diameter (AD) of grown CNTs on different catalysts.

Catalyst Designation	2F	1F1C	2C	1C1N	2N	1F1N
AD of CNTs (nm)	60	39	42	39	44	43

Fig.5 shows the TEM images of CNTs synthesized on 1F1C catalyst sample. Generally, it reveals the hollow core and tubular structure of the grown carbon products which confirms the filamentous morphologies seen in SEM observation are carbon nanotubes and not carbon fibers. The synthesized carbon nanotubes have often straight or curved structures (Fig 5a), however some helicoidal nanotubes can be observed in the final carbon deposit as indicated with red arrow in Fig. 5b. TEM observation revealed that the produced MWCNTs, with diameter ranging from 8 to 34 nm, have wall thickness of 3–29 nm and constructed by 9–85 layers of graphene sheets.

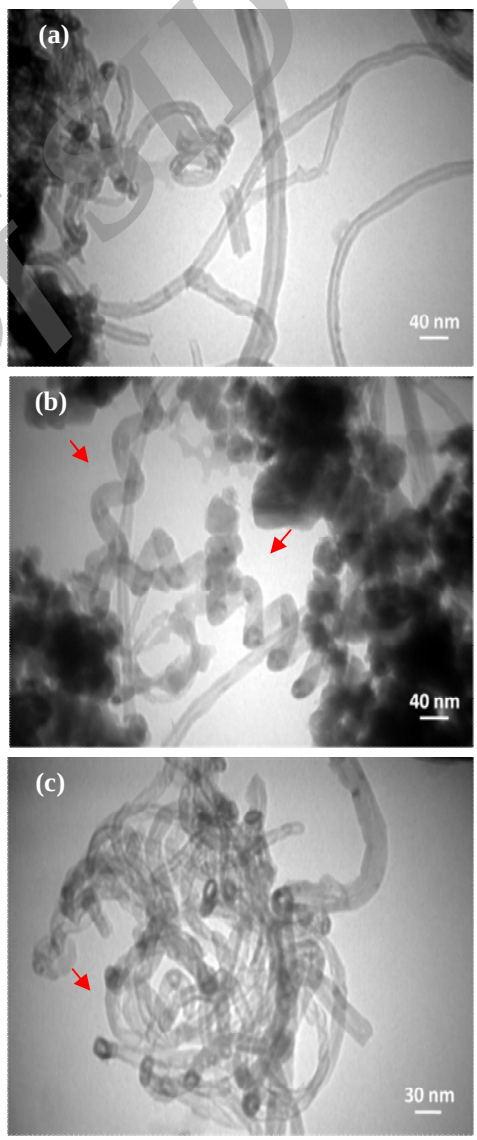

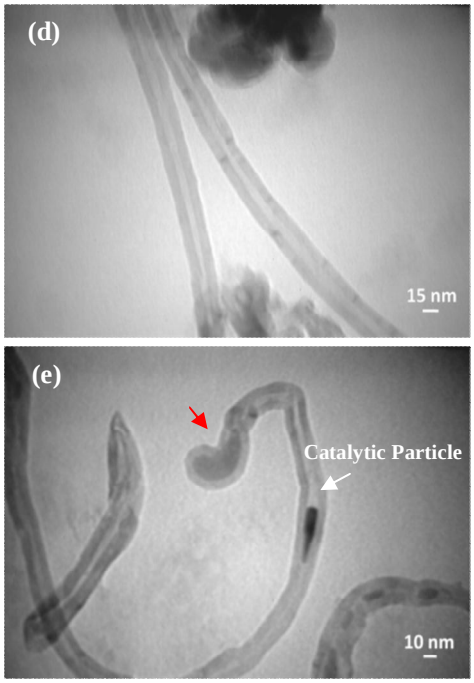

Fig. 5. TEM images of the CNTs synthesized on 1F1C catalyst sample.

It is widely accepted that two growth mechanisms exist for CNT formation: (a) tip-growth model and (b) base-growth model. When the catalyst–substrate interaction is weak (metal has an acute contact angle with the substrate), hydrocarbon decomposes on the top surface of the metal, carbon diffuses down through the metal, and CNT precipitates out across the metal bottom, pushing the whole metal particle off the substrate. This is known as "tip-growth model" [17]. In the other case, when the catalyst–substrate interaction is strong (metal has an obtuse contact angle with the substrate), initial hydrocarbon decomposition and carbon diffusion take place similar to that in the tip-growth case, but the CNT precipitation fails to push the metal particle up; so the precipitation is compelled to emerge out from the metal's apex (farthest from the substrate, having minimum interaction with the substrate). Subsequent hydrocarbon deposition takes place on the lower peripheral surface of the metal, and as dissolved carbon diffuses upward. Thus CNT grows up with the catalyst particle rooted on its base; hence, this is known as "base-growth model" [18]. The red arrows in Fig. 5(c) and 5(e) show the presence of catalyst particles at the tips of CNTs indicating the "tip-growth model". The darker part in Fig 5(e) shown by white arrow is catalytic nanoparticle that was stuck inside carbon nanotube.

The quality and crystalline perfection of the prepared CNTs can also be estimated by Raman spectroscopy [19]. Fig. 6 represents the Raman spectra of grown CNTs on 2F, 1F1C and 2C catalysts. The Raman band appearing in 1500-1605 cm^{-1} region of the wave number is attributed to G band (graphite band) and the one appearing in 1250-1450 cm^{-1} spectral region is known as D band (disorder-induced band) [20]. The G and D bands are characteristic of sp^2–carbon systems: the G vibration is due to the in plane bond stretching motion of carbon pairs whereas the D one is a breathing mode of six fold rings and becomes active only in disordered systems [21].

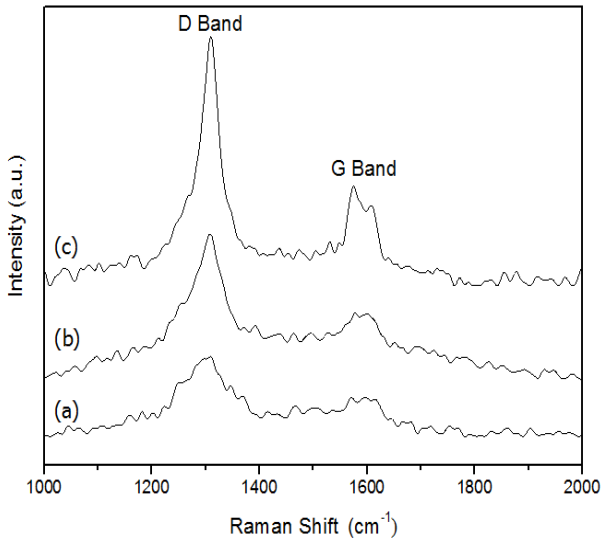

Fig. 6. Raman spectra of CNTs grown on (a) 2F, (b) 1F1C, (c) 2C catalysts**.**

Table 4. Raman I_G/I_D ratio of the synthesized CNTs on three types of prepared catalysts.

Catalyst Designation	2F	1F1C	2C
I_G/I_D of grown CNT	0.49	0.47	0.40

The intensity ratio of G-band to D-band; I_G/I_D indicates the quality and crystallinity of the produced CNTs which is exhibited in table4. The CNTs grown on 2F and 1F1C catalysts have roughly similar qualities, so they have approximately the same level of defects.

4. Conclusion

Thermal CVD was employed to synthesize carbon nanotubes using monometallic and bimetallic combinations of Fe, Co and Ni supported on nanometric SiC as catalysts from acetylene decomposition at 850°C for 15min. The successful growth of nanotubes showed that nanometric SiC powder can be applied as an appropriate substrate for growth of CNTs by CVD. The results showed that on nanometric SiC support, iron oxide nanoprticles show very better efficiency and higher catalytic activity for CNT production compared to cobalt oxide and nickel oxide nanoparticles. It was observed that the best bimetallic composition of the three Fe, Co and Ni metals is Fe-Co which leads to maximum gain of CNT production with smallest average diameter.

References

[1] S. Iijima, nature 354 (1991) 56-58.

[2] X. Hu, S. Cook, P. Wang, H. M. Hwang, X. Liu, Q. L. Williams, Sci. Total Environ. 408 (2010) 1812-1817.

[3] R. H. Baughman, A. A. Zakhidov, W. A. de Heer, Sci. 297 (2002) 787-792.

[4] R. H. Baughman, Sci. 300 (2003) 268-269.

[5] X. Li, H. Zhu, B. Jiang, J. Ding, C. Xu, D. Wu, Carbon 41 (2003) 1664-1666.

[6] W. Jiang, P. Molian, H. Ferkel, J. manuf. Sci. Eng. 127 (2005) 703-707.

[7] C. J. Lee, S. C. Lyu, Y. R. Cho, J. H. Lee, K. I. Cho, Chem. Phys. Lett. 341 (2001) 245-249.

[8] G. Gulino, R. Vieira, J. Amadou, P. Nguyen, M. J. Ledoux, S. Galvagno, C. Pham-Huu, Appl. Catal. A: Gen. 279 (2005) 89-97.

[9] G. H. Jeong, N. Olofsson, L. K. Falk, E. E. Campbell, Carbon 47 (2009) 696-704.

[10] M. Kumar, Y. Ando, J. Nanosci. nanotechno. 10 (2010) 3739-3758.

[11] S. D. Ali, S. T. Hussain, S. R. Gilani, Appl. Surf. Sci. 271 (2013) 118-124.

[12] L. Ci, Z. Ryu, N. Y. Jin-Phillipp, M. Rühle, Diam. Relat. Mater. 16 (2007) 531-536.

[13] T. Murakami, T. Sako, H. Harima, K. Kisoda, K. Mitikami, T. Isshiki, Thin solid films 464 (2004) 319-322.

[14] S. Zhan, Y. Tian, Y. Cui, H. Wu, Y. Wang, S. Ye, Y. Chen, China Particuology 5 (2007) 213-219.

[15] C. Klinke, J. M. Bonard, K. Kern, Surf. Sci. 492 (2001) 195-201.

[16] K. Hernadi, A. Fonseca, J. B. Nagy, A. Siska, I. Kiricsi, Appl. Catal. A: gen. 199 (2000) 245-255.

[17] R. T. K. Baker, M. A. Barber, P. S. Harris, F. S. Feates, R. J. Waite, J. catal. 26 (1972) 51-62.

[18] R. T. K. Baker, R. J. Waite, J. Catal. 37 (1975) 101-105.

[19] H. Hiura, T. W. Ebbesen, K. Tanigaki, H. Takahashi, Chem. Phys. Lett. 202 (1993) 509-512.

[20] M. S. Dresselhaus, G. Dresselhaus, R. Saito, A. Jorio, Phys. Rep. 409 (2005) 47-99.

[21] S. Botti, R. Ciardi, L. Asilyan, L. D. Dominicis, F. Fabbri, S. Orlanducci, A. Fiori, Chem. Phys. Lett. 400 (2004) 264-267.